Multiscale modelling of graphene platelets-based nanocomposite materials

Wiyao Leleng Azoti, Ahmed Elmarakbi

Multiscale modelling of graphene platelets-based nanocomposite materials

Wiyao Leleng Azoti*, Ahmed Elmarakbi

Automotive Composites Group, Faculty of Engineering and Advanced Manufacturing, University of Sunderland, SR6 0DD, United Kingdom

Abstract

This work presents a multiscale framework for the elasto-plastic response of platelets-like inclusions reinforced nanocomposite materials. The solution of the heterogeneous material problem is solved by a kinematic integral equation. An imperfect interface is introduced between the particles and the matrix through a linear spring model LSM, leading to a modified Eshelby's tensor. The interfacial contribution, related to the strain concentration tensor within each material phase and inside the average strain field, is described by a modified Mori-Tanaka scheme. The non-linear response is established in the framework of the J_2 flow rule. An expression of the algorithmic tangent operator for each phase is obtained and used as an uniform modulus for homogenisation purpose. Numerical results are conducted on graphene platelets GPL-reinforced polymer PA6 composite for several design parameters such as GPL volume fraction, aspect ratio and the interfacial compliance. These results clearly highlight the impact of the aspect ratio as well as the volume fraction by a softening in the overall response when imperfection is considered at the interface. Finally, a multiscale simulation is performed on a three bending specimen showing the capability of the developed constitutive equations to be implemented in a finite element FE code.

Keywords: Interfacial imperfection, Graphene platelets, Micromechanics, Modified Eshelby's tensor, Modified Mori-Tanaka scheme, FE simulation

1. Introduction

Nanocomposites have gained worthy significance with use of multifunctional nano fillers like the graphene. This latter finds direct applications in composites. Kuilla et al [1] reported graphene-based polymer composites in which substantial property enhancements have been noticed at much lower volume fraction with respect to polymer composites containing conventional micron-scale

*Corresponding author. Tel. +44 191 515 2684
Email address: Wiyao.Azoti@sunderland.ac.uk (Wiyao Leleng Azoti)

fillers (such as glass or carbon fibres). Graphene has been used to enhance mechanical properties of metal matrix composites [2] for instance in aluminum composite materials where a small amount of graphene nanosheets GNS or even reduced graphene oxide rGO could therefore increase the overall composite physical properties greatly [3]. From a multiscale view point, an approach, for deriving such properties, lies in the combination of molecular mechanics theories and continuum models. The graphene properties are often derived at atomistic scale and the nano particles are treated as equivalent continuum particles [4, 5] that are embedded in the matrix phase through conventional homogenisation techniques.

Despite graphene has been used to increase stiffness, toughness and thermal conductivity of polymer resins by a large margin [6–9], there are still much technological challenges to overcome mainly in the material modelling. This is characterised by the lack of sufficient knowledge on graphene composites for structural applications describing interfacial properties between graphene and polymer matrix under severe loading conditions. It is well-known that the interface characterises the load transfer between the particles/fibres and the matrix. Therefore, it represents an influential parameter that can significantly change the overall properties. Indeed, interface is subjected to defects (debonding, dislocations and cracks) between reinforcements and the matrix and can be identified as one of the predominant damage mechanics in particle and fibre-reinforced composites [10].Then, the accuracy of the composite response needs a proper accounting for the properties of the interface. Several micromechanics models have been developed for that purpose. Among them, one can distinguish the interphase models as well as interface models. The firsts i.e the interphase models introduce the interfacial zone as a layer (with a given tickness and properties) between the particle or fibres and the matrix. First interphase model known as "'three-phase model"' are due to Walpole [11] and then followed by works by Christensen and Lo [12], Hervé and Zaoui [13], Cherkaoui et al. [14] and Lipinski et al. [15]. The seconds i.e the interface models introduce discontinuites in the displacement and/or stress fields at the interface. One can refer to cohesive zone models CZM (Matous and Guebelle [16], Inglis et al. [17], Tan et al. [18, 19]), free sliding model FSM (Ghahremani [20]) and interface stress model ISM (Sharma et al. [21], Sharma and Ganti [22],Sharma and Wheeler [23], Duan et al. [24, 25]) as well as linear spring model LSM (Hashin [26, 27], Qu [28, 29], Zhong and Meguid [30]). Other models for instance, the Gurtin-Murdoch model in works by Nazarenko et al.[31] as well as the discolation-like approach in works by Yu et al. [32, 33] and finally the equivalent inclusion concept in works by Zhao and Weng [34, 35] which later have been used by Yanase and Ju [10] to study the damage

response of spherical particles reinforced composites, should be cited.

This work aims to analyse the effect of an imperfect interface on the non linear response of graphene platelets GPL composite materials. The properties of the GPL which have been widely derived at atomistic scale are not the scope of this work. Herein, advantage is taken of these derivations by considering GPL as continuum phases interacting with the polymer matrix through a slightly weakened interface. The LSM model is then considered for its simplicity and flexibility to treat imperfect interface with limited number of model parameters [10]. The solution of the heterogeneous material problem is obtained by the kinematic integral equation of Dederichs and Zeller [36]. The non linear framework, which is that recently used by Azoti et al. [37, 38], is based on a Hill-type incremental formulation and the classical J_2 flow rule. Therefore, for each phase, the consistent (algorithmic) tangent operator is obtained from the continuum (elasto-plastic) tangent operator and thus from works by Doghri and Ouaar [39]. By accounting for the contribution of the interface, on the one hand inside the strain concentration tensor of the inclusions through the modified Eshelby tensor [28, 29], and on the other hand in the average strain field , a modified version of the Mori-Tanaka is derived for the effective properties.

The paper is organised as follows: section 2 establishes the general framework of a multiscale homogenisation by deriving the global strain concentration tensor; in section 3, the algorithmic tangent operators deriving from the classical J_2 flow theory are recalled. Section 4 gives expressions of the imperfect interface in terms of traction and displacements as well as the modified Eshelby's tensor while section 5 derives the modified Mori-Tanaka scheme for overall responses. The model predictions are therefore compared with open literature data in section 6 where a systematic analysis of micro parameters (aspect ratio, volume fraction, interfacial compliance) is carried out for a GPL-reinforced polymer PA6 under uniaxial tests. Finally, a finite element FE multiscale simulation is performed to illustrate the capabilities of the developed constitutive equations to simulate a macro model structure.

2. Methodology of the multiscale homogenisation

2.1. Kinematic integral equation

Let us consider a composite material consisting of $N+1$ phases. The matrix (phase 0) can be a specific constituent containing all remaining phases. To study this composite, a Representative

Volume Element (RVE) is considered as illustrated by Figure 1. On the RVE boundaries, admissible macroscopic static or kinematic loads are applied in the absence of body forces and inertia terms. The micromechanics scale transition consists, firstly, in the localization of the macroscopic strain tensor $\mathbf{E}$ through a fourth order global strain concentration tensor $\mathbf{A}(r)$ and, secondly, in the homogenisation, which uses averaging techniques to approximate the macroscopic behaviour. Note that $\mathbf{A}(r)$ remains the unknown parameter that contains all the information about the microstructure. The effective properties of the RVE are given by:

$$\mathbf{C}^{eff} = \frac{1}{V}\int_V \mathbf{c}(r) : \mathbf{A}(r) dV \tag{1}$$

where $\mathbf{c}(r)$ denotes the local uniform modulus and V the volume of the RVE. The operator ":"

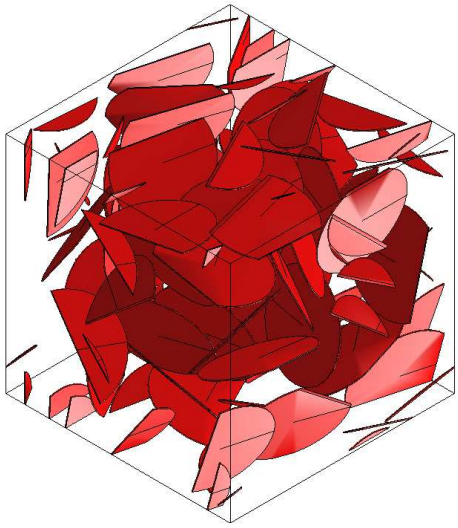

Figure 1: Illustration of platelets-like inclusions reinforced 3D random RVE.

stands for the tensorial contraction over two indices. The global strain concentration tensor $\mathbf{A}(r)$ links the local strain $\boldsymbol{\epsilon}(r)$ to the macroscopic strain $\mathbf{E}$ as follows:

$$\boldsymbol{\epsilon}(r) = \mathbf{A}(r) : \mathbf{E} \tag{2}$$

The decomposition of the local uniform modulus into a homogeneous reference part $\mathbf{c}^R$ and a fluctuation part $\delta\mathbf{c}$ such as:

$$\mathbf{c}(r) = \mathbf{c}^R(r) + \delta\mathbf{c}(r) \tag{3}$$

Equation (3) enables the derivation of the kinematic integral equation of Dederichs and Zeller [36]. In terms of strain fields, the kinematic integral equation reads:

$$\boldsymbol{\epsilon}(r) = \mathbf{E}^R(r) - \int_V \boldsymbol{\Gamma}(r - r') : \delta\mathbf{c}(r') : \boldsymbol{\epsilon}(r') dV' \tag{4}$$

where $\mathbf{E}^R(r)$ is the strain field inside the reference infinite medium and $\mathbf{\Gamma}(r-r')$ is the modified Green tensor.

2.2. Global strain concentration tensor based on Eshelby's ellipsoidal inclusion

The kinematic integral equation (4) represents the formal solution the global strain concentration tensor is derived from. Based on an iterative procedure proposed by Vieville et al. [40], the global strain concentration tensor $\mathbf{A}^I(r)$ for a I^{th} phase of the RVE is given as:

$$\begin{cases} \mathbf{A}^I(r) = \mathbf{a}^I(r) : (\bar{\mathbf{a}}^I(r))^{-1} \\ \bar{\mathbf{A}}^I(r) = \mathbf{I} \end{cases} \tag{5}$$

$\mathbf{I}$ represents the fourth order symmetric identity tensor and $\bar{\bullet}$ is the mean-field volume average of $\bullet$. The quantity $\mathbf{a}^I(r)$ is the local strain concentration tensor with respect to the reference medium such that:

$$\boldsymbol{\epsilon}^I(r) = \mathbf{a}^I(r) : \mathbf{E}^R \tag{6}$$

The I^{th} concentration tensor $\mathbf{a}^I$ is given by:

$$\begin{cases} \mathbf{a}_0^I(r) = \mathbf{I} \\ \mathbf{a}_{i+1}^I(r) = [\mathbf{I} + \mathbf{T}^{II} : (\mathbf{c}^I(r) - \mathbf{c}^R(r))]^{-1} : [\mathbf{I} - \sum_{J=0, J\neq I}^{N} \mathbf{T}^{IJ} : (\mathbf{c}^J(r) - \mathbf{c}^R(r)) : \mathbf{a}_i^J(r)] \\ I = 0, 1, 2, ..., N \end{cases} \tag{7}$$

with N the number of phases considered in the composite. In equation (7), $\mathbf{a}_i^I(r)$ represents an approximation of the I^{th} concentration tensor at iteration i. $\mathbf{T}^{II}$ and $\mathbf{T}^{IJ}$ are the interaction tensors in one-site (OS) and multi-site (MS) versions, respectively. Their general expression is:

$$\mathbf{T}^{IJ} = \frac{1}{V_I} \int_{V_I} \int_{V_J} \mathbf{\Gamma}(r-r') dV dV' \tag{8}$$

The computational framework of $\mathbf{T}^{II}$ and $\mathbf{T}^{IJ}$ is proposed by Fassi-Fehri [41].

Let us suppose that the geometry of any phase within the RVE is ellipsoidal. The Eshelby's inclusion concept [42] assumes that the strain field inside an ellipsoidal inclusion is uniform. Therefore, a characteristic function $\theta(r)$ can be defined such as [40]:

$$\theta(r) = \begin{cases} 1 & \text{if } r \in V_I \\ 0 & \text{if } r \notin V_I \end{cases} \tag{9}$$

Based on equation (9) and the average strain field within an inclusion I such as:

$$\boldsymbol{\epsilon}^I = \frac{1}{V_I}\int_{V_I} \boldsymbol{\epsilon}\left(\mathbf{r}\right) dV \tag{10}$$

the above kinematic integral equation (4) can be rewritten as:

$$\boldsymbol{\epsilon}^I = \mathbf{E}^R - \sum_{J=0}^{N} \mathbf{T}^{IJ} : (\mathbf{c}^J - \mathbf{c}^R) : \boldsymbol{\epsilon}^J \text{ with } I = 0, 1, 2, ..., N \tag{11}$$

and the local concentration tensor Eq.(7) becomes:

$$\begin{cases} \mathbf{a}_0^I = \mathbf{I} \\ \mathbf{a}_{i+1}^I = [\mathbf{I} + \mathbf{T}^{II}(\mathbf{c}^R) : (\mathbf{c}^I - \mathbf{c}^R)]^{-1} : [\mathbf{I} - \sum_{J=1, J\neq I}^{N} \mathbf{T}^{IJ} : (\mathbf{c}^J - \mathbf{c}^R) : \mathbf{a}_i^J] \\ I = 0, 1, 2, ..., N \end{cases} \tag{12}$$

In the case of OS version (most frequent developments in the literature) and for isotropic medium, the interaction tensor $\mathbf{T}^{II}$ can be deduced from the Eshelby's tensor $\mathbf{S}$ such as $\mathbf{T}^{II} = \mathbf{S} : (\mathbf{c}^R)^{-1}$. In such condition and neglecting the interactions among inclusion I and its neighbours J, i.e. all the tensors $\mathbf{T}^{IJ} = 0$, the local concentration tensor $\mathbf{a}^I$ reads more simple expression:

$$\mathbf{a}^I = [\mathbf{I} + \mathbf{S} : (\mathbf{c}^R)^{-1} : (\mathbf{c}^I - \mathbf{c}^R)]^{-1} \text{ with } I = 0, 1, 2, ..., N \tag{13}$$

Finally, the global strain concentration tensor $\mathbf{A}^I$ is calculated by substituting equation (13) in (5). Therefore, for any homogenization model defined by $\mathbf{A}^I$, the effective or macro-stiffness tensor $\mathbf{C}^{eff}$ is given through a discrete form of the equation (1) by:

$$\mathbf{C}^{eff} = \sum_{I=0}^{N} f_I \mathbf{c}^I : \mathbf{A}^I. \tag{14}$$

with the volume fraction f_I defined as:

$$f_I = \frac{V_I}{V} \tag{15}$$

3. Non-linear tangent operators

Let us consider that one or more phases behave elasto-plastically within the RVE. Referring to the work of Doghri and Ouaar [39], at least two tangent operators can be defined: the "continuum" (or elasto-plastic) $\mathbf{C}^{ep}$ tangent operator, which is derived from the rate constitutive equation, and the "consistent" (or algorithmic) $\mathbf{C}^{alg}$ tangent operator, which is solved from a discretisation of the rate equation in time interval $[t_n, t_{n+1}]$:

$$\begin{cases} \dot{\boldsymbol{\sigma}} = \mathbf{C}^{ep} : \dot{\boldsymbol{\epsilon}} \\ \delta\boldsymbol{\sigma}_{n+1} = \mathbf{C}^{alg} : \delta\boldsymbol{\epsilon}_{n+1} \end{cases} \tag{16}$$

The explicit expressions of the tangent operators are derived from the classical J_2 flow rule such as:

$$\begin{cases} \mathbf{C}^{ep} = \mathbf{C}^{el} - \frac{(2G)^2}{h}\mathbf{N} \otimes \mathbf{N} \\ h = 3G + \frac{dR}{dp} \end{cases} \tag{17}$$

$$\begin{cases} \mathbf{C}^{alg} = \mathbf{C}^{ep} - (2G)^2 (\Delta p) \frac{\sigma_{eq}}{\sigma_{eq}^{trial}} \frac{\partial \mathbf{N}}{\partial \sigma} \\ \frac{\partial \mathbf{N}}{\partial \sigma} = \frac{1}{\sigma_{eq}} \left(\frac{3}{2}\mathbf{I}_{dev} - \mathbf{N} \otimes \mathbf{N} \right) \end{cases} \tag{18}$$

In equations (17) and (18), G denotes the material shear modulus while the operator "$\otimes$" designates the tensorial product. $\mathbf{C}^{el}$ represents the elastic stiffness tensor and $R(p)$ is the hardening stress with p the accumulated plastic strain. $\mathbf{N}$ represents the normal to the yield surface in the stress space. σ_{eq}^{trial} denotes a trial elastic predictor of σ_{eq}. $\mathbf{I}_{dev}$ stands for the deviatoric part of the fourth order symmetric identity tensor. The knowledge of internal variables such as Δp and σ_{eq}^{trial} remains crucial for computation of the algorithmic tangent operator (18). This tangent operator will be used later as uniform modulus to compute the overall behaviour of the composite in section 5. A detailed procedure about internal variables computation can be found in [38].

4. Imperfect interface and the modified Eshelby's tensor

Let us consider the interface γ between two phases of a composite material. The linear spring model LSM supposes the continuity of the traction vector across the interface while the jump of displacment field is consedered to be proportional to the traction on that interface. These assumption are written like:

$$\begin{cases} \Delta\sigma_{ij} n_j = \left[\sigma_{ij}\left(\gamma^+\right) - \sigma_{ij}\left(\gamma^-\right)\right] n_j = 0 \\ \Delta u_i = \left[u_i\left(\gamma^+\right) - u_i\left(\gamma^-\right)\right] = \eta_{ij}\sigma_{jk} n_k \end{cases} \tag{19}$$

with n_j the components of a unit vector normal to the interface. $u_i\left(\gamma^+\right)$ and $u_i\left(\gamma^-\right)$ stand for the values of $u_i\left(x\right)$ as x reaches the interface from outside and inside of the inclusion respectively. $\sigma_{ij}\left(\gamma^+\right)$ and $\sigma_{ij}\left(\gamma^-\right)$ are the dual in terms of stress. The second order tensor components η_{ij} denote the compliance of the interface. It appears that $\eta_{ij} = 0$ leads to a perfectly bonded interface whereas $\eta_{ij} \longrightarrow \infty$ represents a completely debonded interface. The expression of η_{ij} is given by [28, 29]:

$$\eta_{ij} = \alpha\delta_{ij} + (\beta - \alpha)\, n_i n_j \tag{20}$$

where the constants α and β stand for the extent of interfacial sliding and the interfacial separation, respectively. δ_{ij} is the Kronecker symbol. Indeed, α and β are the parameters related to the

delamination and the debonding at the interface. When LSM is used for an imperfect interface, these parameters can be estimated from the anti-interpenetration model AIM proposed by Wang et al. [43]. Furthermore, works by Hashin [44] has demonstrated that the LSM for interface can accurately approximate the thin and compliant interphase studied in [43].

In the case of ellipsoidal inclusions, Qu [28, 29] has determined the Eshelby's tensor for these inclusions embedded in an elastic matrix and showing a slightly weakened interface i.e when η_{ij} is very small. Therefore, the modified Eshelby's tensor for this problem yields :

$$\mathbf{S^M} = \mathbf{S} + (\mathbf{I} - \mathbf{S}) : \mathbf{H} : \mathbf{c} : (\mathbf{I} - \mathbf{S}) \tag{21}$$

where $\mathbf{S}$ denotes the original Eshelby's tensor [42] and $\mathbf{H}$ stands for a four order tensor depending on the interface properties and the geometry of the inclusion. Expressions of components of tensor $\mathbf{H}$ for ellipsoidal inclusions are given by:

$$H_{ijkl} = \alpha P_{ijkl} + (\beta - \alpha)\, Q_{ijkl} \tag{22}$$

where P_{ijkl} and Q_{ijkl} are given for ellipsoidal inclusions by:

$$\begin{cases} P_{ijkl} = \frac{3}{16\pi} \int_0^{\pi} \left[\int_0^{2\pi} \left(\delta_{ik} n_j n_l + \delta_{jk} n_i n_l + \delta_{il} n_k n_j + \delta_{jl} n_k n_i \right) \mathbf{n}^{-1} d\theta \right] sin\phi d\phi \\ Q_{ijkl} = \frac{3}{4\pi} \int_0^{\pi} \left[\int_0^{2\pi} \left(n_i n_j n_k n_l \right) \mathbf{n}^{-3} d\theta \right] sin\phi d\phi \\ \mathbf{n} = \left(n_i n_i \right)^{1/2} \\ n = \left(\frac{sin\phi cos\theta}{a_1}; \frac{sin\phi sin\theta}{a_2}; \frac{cos\theta}{a_3} \right)^{\mathbf{T}} \end{cases} \tag{23}$$

In others terms, Eq. (21) can be written such as:

$$S^{\mathbf{M}}_{ijkl} = S_{ijkl} + \left(I_{ijpq} - S_{ijpq} \right) H_{pqrs} c_{rsmn} \left(I_{mnkl} - S_{mnkl} \right) \tag{24}$$

5. Modified Mori-Tanaka scheme for overall responses

General considerations on Mori-Tanaka scheme can be found in works by Azoti et al. [37]. Therefore, the MT effective properties are given by:

$$\mathbf{C^{MT}} = \sum_{I=0}^{N} f_I \mathbf{c}^I : \mathbf{A}^I = \left(f_0 \mathbf{c}^0 + \sum_{J=1}^{N} f_I \mathbf{c}^I : \mathbf{a}^I \right) : \mathbf{A}^0 \tag{25}$$

with $\mathbf{A}^0$ the global strain concentration of the matrix. By accounting for the interface contributions, modifications come out with the definition of the average strain field:

$$\mathbf{E} = \frac{1}{V} \int_V \boldsymbol{\epsilon}\left(\mathbf{x}\right) dV = \sum_{I=0}^{N} f_I \boldsymbol{\epsilon}^I + \frac{1}{V} \int_{\gamma} \frac{1}{2} \left(\Delta \mathbf{u} \otimes \mathbf{n} + \mathbf{n} \otimes \Delta \mathbf{u} \right) dS \tag{26}$$

where γ represents the union of all interfaces. The combination of Eq.(19)-b and Eq.(26) leads to the following expression of the average strain:

$$\mathbf{E} = \sum_{I=0}^{N} f_I \boldsymbol{\epsilon}^I + \frac{1}{V} \sum_{I=1}^{N} \int_{\gamma_I} \frac{1}{2} \left[(\boldsymbol{\eta}.\boldsymbol{\sigma}.\mathbf{n}) \otimes \mathbf{n} + \mathbf{n} \otimes (\boldsymbol{\eta}.\boldsymbol{\sigma}.\mathbf{n}) \right] dS \tag{27}$$

with γ_I the surface of the volume V_I.

The evaluation of the integral terms in Eq.(27) remains tricky for an arbitrary interface geometry. However by taking advantage of developments by Qu [28] for slightly weakened interface, the stress distribution on the surface γ_I can be replaced by its average over the volume V_I leading to a simplified form of Eq.(27) such as:

$$\mathbf{E} = \sum_{I=0}^{N} f_I \boldsymbol{\epsilon}^I + \sum_{I=1}^{N} f_I \mathbf{H}^I : \boldsymbol{\sigma}^I \tag{28}$$

Using Eq.(5) and derivations in [37], one can demonstrate the following relationship between the average strain within an inclusion and the matrix such as:

$$\boldsymbol{\epsilon}^I = \mathbf{a}^I : \boldsymbol{\epsilon}^0 \tag{29}$$

where $\mathbf{a}^I$ in the OS-version yields:

$$\mathbf{a}^I = [\mathbf{I} + \mathbf{S}^{\mathbf{M}} : (\mathbf{c}^R)^{-1} : (\mathbf{c}^I - \mathbf{c}^R)]^{-1} \text{ with } I = 1, 2, ..., N \tag{30}$$

Combining Eq.(29) and Eq.(28) leads to

$$\mathbf{E} = \left[\sum_{I=0}^{N} f_I \mathbf{a}^I + \sum_{I=1}^{N} f_I \mathbf{H}^I : \mathbf{c}^I : \mathbf{a}^I \right] : \boldsymbol{\epsilon}^0 \tag{31}$$

The inversion of Eq.(28)

$$\boldsymbol{\epsilon}^0 = \left[\sum_{I=0}^{N} f_I \mathbf{a}^I + \sum_{I=1}^{N} f_I \mathbf{H}^I : \mathbf{c}^I : \mathbf{a}^I \right]^{-1} : \mathbf{E} \tag{32}$$

in conjunction with Eq.(2) leads to the modified global concentration tensor of the matrix $\mathbf{A}^0$ such as:

$$\mathbf{A}^0 = \left[\sum_{I=0}^{N} f_I \mathbf{a}^I + \sum_{I=1}^{N} f_I \mathbf{H}^I : \mathbf{c}^I : \mathbf{a}^I \right]^{-1} \tag{33}$$

Substituting Eq.(33) into Eq.(25) gives the modified Mori-Tanaka effective properties such as:

$$\mathbf{C}^{\mathbf{MT}}_{modified} = \left(f_0 \mathbf{c}^0 + \sum_{I=1}^{N} f_I \mathbf{c}^I : \mathbf{a}^I \right) : \left[\sum_{I=0}^{N} f_I : \mathbf{a}^I + \sum_{I=1}^{N} f_I \mathbf{H}^I : \mathbf{c}^I : \mathbf{a}^I \right]^{-1} \tag{34}$$

In the case a 2-phase composite, Eq.(34) yields

$$\mathbf{C}^{\mathbf{MT}}_{modified} = \left(f_0 \mathbf{c}^0 + f_I \mathbf{c}^I : \mathbf{a}^I \right) : \left[f_0 \mathbf{I} + f_I \left(\mathbf{I} + \mathbf{H}^I : \mathbf{c}^I \right) : \mathbf{a}^I \right]^{-1} \tag{35}$$

6. Numerical simulations

6.1. Model validations

The capability of the present model to reproduce results from the open literature is carried out herein. In a first instance, the model predictions are compared with the earlier works by Qu [28]. Let us consider a composite consisting of an isotropic matrix and aligned isotropic ellipsoidal inclusions (a_1, a_2, a_3) with aspect ratio AR such as $AR = \frac{a_3}{a_1}$ and $a_1 = a_2 = a$. A pure sliding case is considered i.e $\alpha \neq 0$ and $\beta = 0$. The sliding interfacial separation constant α is given such as $\alpha = a\alpha_0/\mu_M$ with α_0 the sliding coefficient and a the ellipsoid semi-axis. The material properties for this analysis are gathered in Table 1.

Matrix		Inclusions				
μ_0 [GPa]	ν_0	μ_I [GPa]	ν_I	AR	α	β
1.0	0.4	30	0.25	2.0	$a\alpha_0/\mu_M$	0.0

Table 1: Material properties from works by Qu [28]

Figure 2 shows the evolution of the normalised effective transverse ans longitudinal Young modulus E_{11}/μ_0 and E_{33}/μ_0 as well as the effective longitudinal Poisson's ratio ν_{31} versus the volume fraction of the inclusions. These predictions are concerned with the originate Mori-Tanaka scheme for perfect bonded inclusions denoted "*MT*", the originate MT using only the modified Eshelby's tensor denoted "*MT*, $\alpha_0 = 0.3$" and finally the modified MT using the modified Eshelby's tensor denoted "*Modif. MT*, $\alpha_0 = 0.3$". Different trends are obtained for the Young moduli and the Poisson's ratio. Indeed, the higher the inclusions volume fraction, the higher the Young moduli E_{11}/μ_0 and E_{33}/μ_0. However, accounting for a pure sliding interface has led to a decrease of the effective stiffness. For the Poisson's ratio ν_{31}, when a decrease is noticed for others methods i.e *MT* and *Modif. MT*, $\alpha_0 = 0.3$, a parabolic trend is observed when a weakened interface *Modif. MT*, $\alpha_0 = 0.3$ is accounting for with a minimum at $f_I = 0.3$. A fair agreement is found between the present predictions with respect to results by Qu [28] showing by the way the effectiveness of the numerical integration method used for solving equations (23).

6.2. GPL-reinforced polymer PA6 composite materials

As application of the present development to polymer composite, a GPL reinforced PA-6 polymer matrix is considered. Due to its hexagonal atomic structure, the graphene can display an

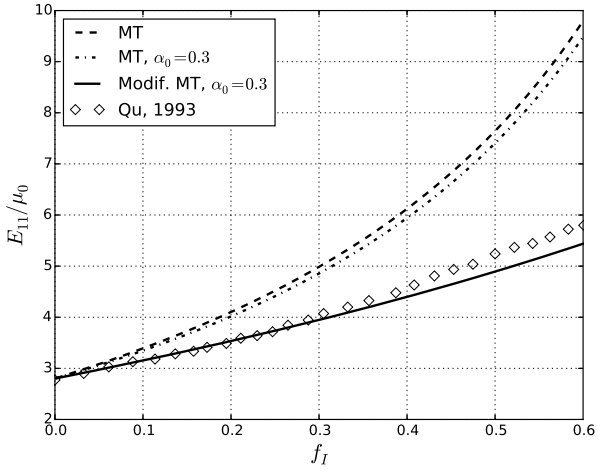

(a) E_{11}/μ_0

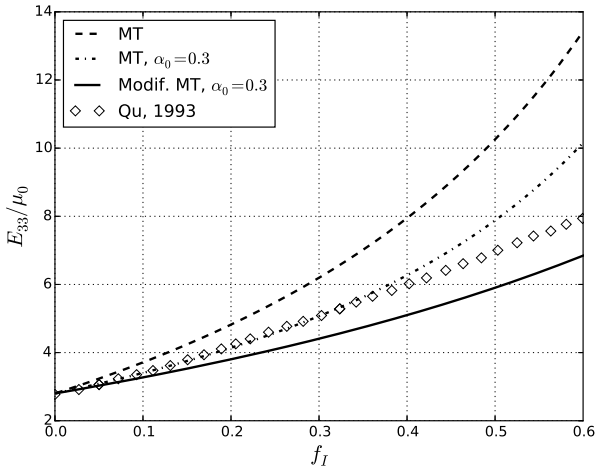

(b) E_{33}/μ_0

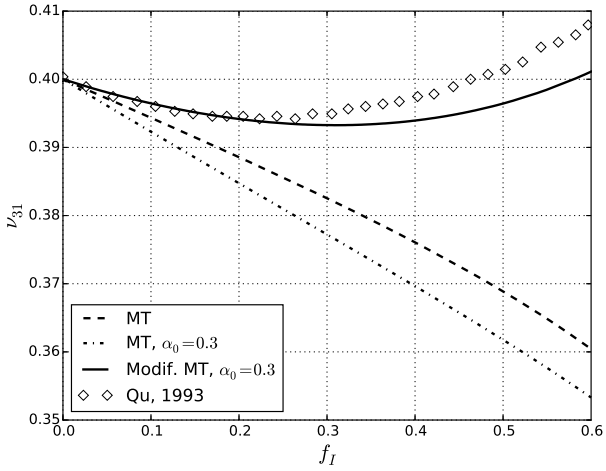

(c) ν_{31}

Figure 2: Effective elastic moduli of ellipsoidal inclusions reinforced composite

anisotropic behaviour as described by Shokriech et al. [45]. Moreover, it can also undergo a non-linear elastic behaviour. This has been recently studied by Elmarakbi et al.[46]. However, the dominant mechanical properties of graphene remain the in-plane behaviour which has been demonstrated to be isotropic in works by Cho et al. [5]. Therefore, an elastic and isotropic behaviour is considered for the GPL. The PA-6 matrix is considered elasto-plastic with an isotropic hardening power law defined as $R(r) = hr^m$. The material properties is presented in Table 2. The macro stress-strain response is studied under uniaxial loading. The loading is given in terms of a macro stain increment $\Delta\mathbf{E} = \Delta E\ \mathbf{\Psi}$ with $\mathbf{\Psi} = \mathbf{e}_1 \otimes \mathbf{e}_1 - \frac{1}{2}(\mathbf{e}_2 \otimes \mathbf{e}_2 + \mathbf{e}_3 \otimes \mathbf{e}_3)$. The effective response of the composite is assessed through different design parameters for instance the platelets aspect ratio AR, the volume fraction f_I and the interface sliding coefficient α_0.

Matrix					Inclusions	
E_0 [GPa]	ν_0	σ_Y [MPa]	h [MPa]	m	E_I [GPa]	ν_I
2.0	0.39	60.5	63	0.4	1000	0.22

Table 2: Material properties for GPL/PA-6 composite materials

Figure 3-a shows the evolution of the equivalent stress-strain response versus the AR. This parameter has a significant impact on the effective response. Indeed, an increase of the effective stiffness is noticed with the decrease of the AR. Lower values such as $AR = 10^{-1}$ corresponding to platelets-like shape show more effective reinforcement character than circular-like shape i.e $AR = 1$.

In addition, the variation of the volume fraction f_I is analysed in Figure 3-b. The predictions reproduce a trend similar to the matrix for $f_I = 0$ and subsequently shifts towards higher stress with the increase of f_I. The influence of the interface imperfection is analysed in Figures 4-a and 4-b. the higher the sliding coefficient α_0, the lower and softer the effective stress-strain response as shown by Figure 4-a. In Figure 4-a, the results obtained from a perfect interface and an imperfect interface modelling are compared. the higher the volume fraction, the higher the gap between the two responses and the lower the effective response that accounts for the interface imperfection.

6.3. Multiscale simulation on a three-point bending specimen

The developed constitutive equations are implemented through a multiscale simulation on a three-bending specimen as described by Figure 5. Due to the symmetry of the problem, the sim-

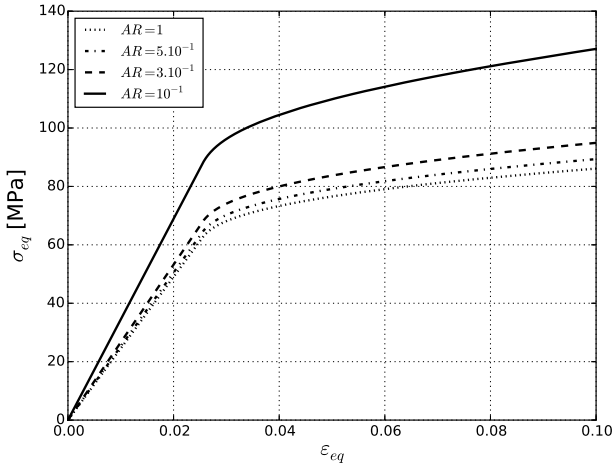

(a) Aspect ratio variation for $f_I = 0.1$ and $\alpha_0 = 0.3$

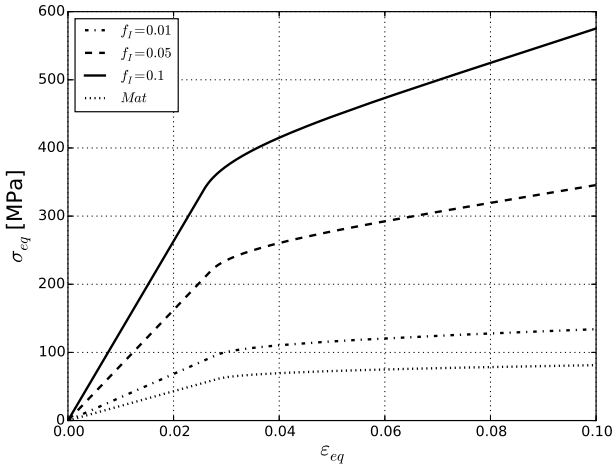

(b) Volume fraction variation for $AR = 10^{-2}$ and $\alpha_0 = 0.3$

Figure 3: Study of design parameters for a GPL/PA-6 composite

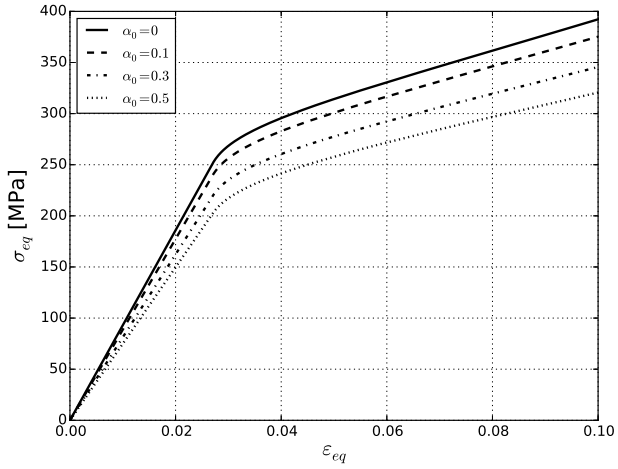

(a) Interface sliding compliance variation for $AR = 10^{-2}$ and for $f_I = 0.05$

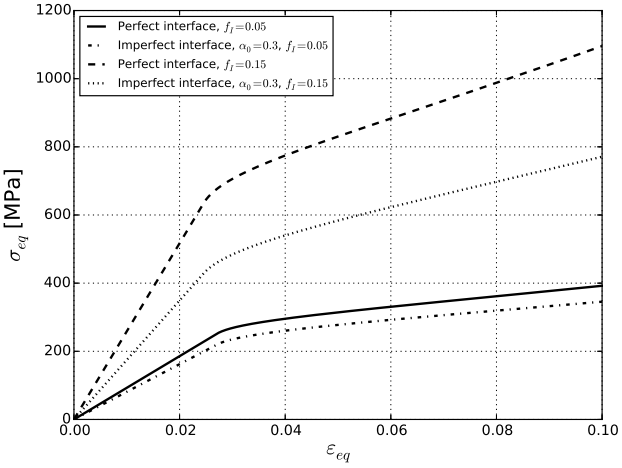

(b) Imperfect versus perfect interface for $AR = 10^{-2}$

Figure 4: Study of interfacial parameters for a GPL/PA-6 composite

ulation is performed on the half of the geometry. The mesh is composed of 1737 CPE4 elements (Figure 6-a). The loading point and the support points for the specimen are simulated by analytical rigid surfaces [47]. A metal matrix Al is considered with an elasto-plastic behaviour while the GPL are assumed isotropic. These material properties are summarised in Table 3. The boundaries conditions are prescribed in terms of displacement at the loading point and enables a postprocessing of the reaction force at that point versus the displacement.

Matrix					Inclusions	
E_0 [GPa]	ν_0	σ_Y [MPa]	h [MPa]	m	E_I [GPa]	ν_I
75.0	0.23	75.0	416	0.3895	1000	0.22

Table 3: Material properties for GPL reinforced MMCs

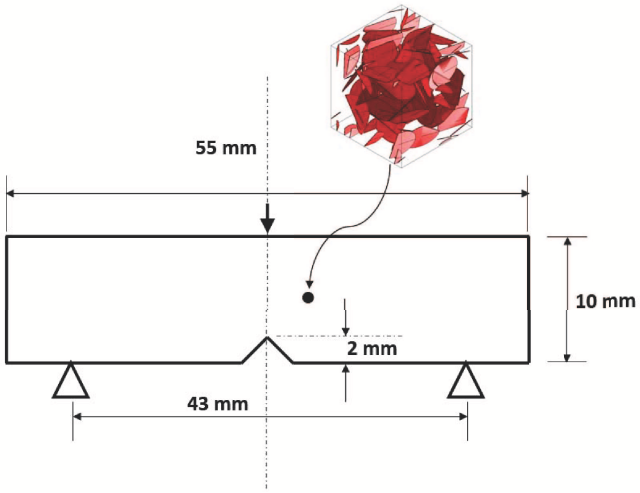

Figure 5: Illustration of a multiscale bending specimen.

Figures 6b-f are concerned with the deformed specimen and show the contour plots of stress, displacement and the accumulated plastic strain p. Figure 7 presents the evolution of the reaction force versus the displacement at the loading point. Two volume fractions are analysed for this GPL reinforced MMC and the simulation predictions are obtained for both the perfect and imperfect cases. One can observe the decrease of the reaction force in the case of imperfect interface. As obtained previously in the above section, the gap between both cases is sensitive to the GPL volume fraction. The lower, the volume fraction, the lower, the gap.

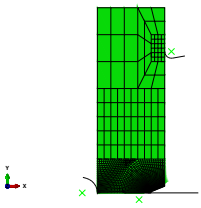

(a) Mesh

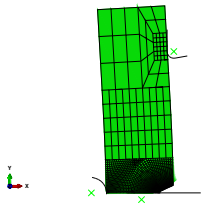

(b) Deformed mesh

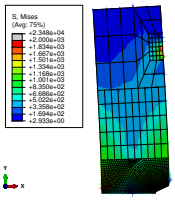

(c) Mises Stress

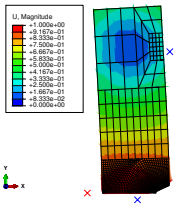

(d) Displacement magnitude

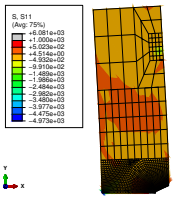

(e) S11, Stress

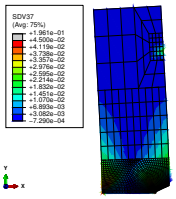

(f) Accumulated plastic strain

Figure 6: Contours plots of the deformed sample for $AR = 10^{-2}$ $f_I = 0.15$ and $\alpha_0 = 0.3$

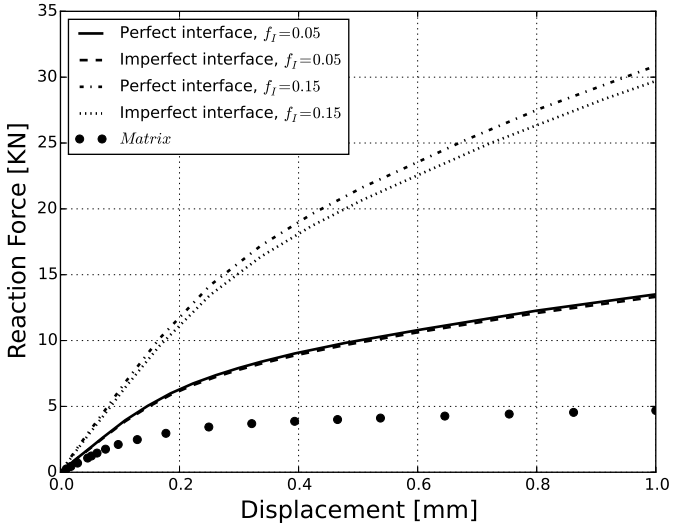

Figure 7: Reaction force versus displacement.

7. Conclusion

The elasto-plastic response of graphene platelets based composites has been analysed regarding the interfacial behaviour. For such a purpose, the linear spring model LSM is considered for its simplicity and flexibility to treat imperfection at the interface with limited number of model parameters. Therefore, a modified expression is obtained for both the Eshelby's tensor and the Mori-Tanaka scheme for deriving the effective response of the composite.

Results carried out on GPL reinforced PA-6 polymer highlight the importance of the aspect ratio. Most effective reinforcement is observed with low value of the aspect ratio. The sliding coefficient also show a significant influence on the overall behaviour along with the volume fraction. Indeed, the higher the volume fraction, the higher the softening in the stress-stress response. The capabilities of the model to be implemented in a FE code is demonstrated on GPL reinforced metal matrix composites.

As an outlook, results of this study are expected to be integrated in the design of new graphene based composite for automotive applications. The influence of the sliding coefficient α_0 in a multi-scale crashworthiness simulation is of interest by studying the strain energy absorption SEA.

8. Acknowledgements

The research leading to these results has received funding from the European Union Seventh Framework Programme under grant agreement No. 604391 and Horizon 2020 Programme under grant agreement No. 696656 Graphene Flagship.

References

[1] T. Kuilla, S. Bhadra, D. Yao, N. H. Kim, S. Bose, J. H. Lee, Recent advances in graphene based polymer composites, Progress in Polymer Science 35 (11) (2010) 1350 – 1375. doi:http://dx.doi.org/10.1016/j.progpolymsci.2010.07.005.

[2] A. F. Boostani, S. Tahamtan, Z. Jiang, D. Wei, S. Yazdani, R. A. Khosroshahi, R. T. Mousavian, J. Xu, X. Zhang, D. Gong, Enhanced tensile properties of aluminium matrix composites reinforced with graphene encapsulated sic nanoparticles, Composites Part A: Applied Science and Manufacturing 68 (2015) 155 – 163. doi:http://dx.doi.org/10.1016/j.compositesa.2014.10.010.

[3] J. Liu, U. Khan, J. Coleman, B. Fernandez, P. Rodriguez, S. Naher, D. Brabazon, Graphene oxide and graphene nanosheet reinforced aluminium matrix composites: Powder synthesis and prepared composite characteristics, Materials & Design 94 (2016) 87 – 94. doi:http://dx.doi.org/10.1016/j.matdes.2016.01.031.

[4] J. Xiao, B. Gama, J. G. Jr., An analytical molecular structural mechanics model for the mechanical properties of carbon nanotubes, International Journal of Solids and Structures 42 (2005) 3075 – 3092. doi:http://dx.doi.org/10.1016/j.ijsolstr.2004.10.031.

[5] J. Cho, J. Luo, I. Daniel, Mechanical characterization of graphite/epoxy nanocomposites by multi-scale analysis, Composites Science and Technology 67 (1112) (2007) 2399 – 2407. doi:http://dx.doi.org/10.1016/j.compscitech.2007.01.006.

[6] M. A. Rafiee, J. Rafiee, I. Srivastava, Z. Wang, H. Song, Z.-Z. Yu, N. Koratkar, Fracture and fatigue in graphene nanocomposites, Small 6 (2) (2010) 179–183. doi:10.1002/smll.200901480.

[7] L. M. Veca, M. J. Meziani, W. Wang, X. Wang, F. Lu, P. Zhang, Y. Lin, R. Fee, J. W. Connell, Y.-P. Sun, Carbon nanosheets for polymeric nanocomposites with high thermal conductivity, Advanced Materials 21 (20) (2009) 2088–2092. doi:10.1002/adma.200802317.

[8] Z. Xu, C. Gao, In situ polymerization approach to graphene-reinforced nylon-6 composites, Macromolecules 43 (16) (2010) 6716–6723. doi:10.1021/ma1009337.

[9] W. L. Zhang, B. J. Park, H. J. Choi, Colloidal graphene oxide/polyaniline nanocomposite and its electrorheology, Chem. Commun. 46 (2010) 5596–5598. doi:10.1039/C0CC00557F.

[10] K. Yanase, J. Ju, Overall elastoplastic damage responses of spherical particle-reinforced composites containing imperfect interfaces, International Journal of Damage Mechanics vol. 23 (no. 3) (2014) 411–429.

[11] L.-J. Walpole, A coated inclusion in an elastic medium, Mathematical Proceedings of the Cambridge Philosophical Society 83 (1978) 495. doi:10.1017/S0305004100054773.

[12] R. M. Christensen, K. H. Lo, Solutions for effective shear properties in three phase sphere and cylinder models, Journal of the Mechanics and Physics of Solids 27 (4) (1979) 315 – 330. doi:DOI:10.1016/0022-5096(79)90032-2.

[13] E. Hervé, A. Zaoui, n-layered inclusion-based micromechanical modelling, International Journal of Engineering Science 31 (1) (1993) 1 – 10. doi:DOI:10.1016/0020-7225(93)90059-4.

[14] M. Cherkaoui, H. Sabar, M. Berveiller, Micromechanical approach of the coated inclusion problem and applications to composite materials, Journal of engineering materials and technology, vol. 116, no 3 (11 ref.), pp. 274-278 (1994).

[15] P. Lipinski, E. Barhdadi, M. Cherkaoui, Micromechanical modeling of an arbitrary ellipsoidal multi-coated inclusion, Philosophical Magazine 86 (10) (2006) 1305–1326.

[16] K. Matous, P. H. Geubelle, Finite element formulation for modeling particle debonding in reinforced elastomers subjected to finite deformations, Computer Methods in Applied Mechanics and Engineering 196 (1-3) (2006) 620 – 633. doi:DOI:10.1016/j.cma.2006.06.008.

[17] H. Inglis, P. Geubelle, K. Matous, H. Tan, Y. Huang, Cohesive modeling of dewetting in particulate composites: micromechanics vs. multiscale finite element analysis, Mechanics of Materials 39 (6) (2007) 580 – 595. doi:http://dx.doi.org/10.1016/j.mechmat.2006.08.008.

[18] H. Tan, Y. Huang, C. Liu, P. Geubelle, The mori-tanaka method for composite materials with nonlinear interface debonding, International Journal of Plasticity 21 (10) (2005) 1890 – 1918. doi:DOI:10.1016/j.ijplas.2004.10.001.

[19] H. Tan, C. Liu, Y. Huang, P. Geubelle, The cohesive law for the particle/matrix interfaces in high explosives, Journal of the Mechanics and Physics of Solids 53 (8) (2005) 1892 – 1917. doi:http://dx.doi.org/10.1016/j.jmps.2005.01.009.

[20] F. Ghahremani, Effect of grain boundary sliding on anelasticity of polycrystals, International Journal of Solids and Structures 16 (9) (1980) 825 – 845. doi:http://dx.doi.org/10.1016/0020-7683(80)90052-9.

[21] P. Sharma, S. Ganti, N. Bhate, Effect of surfaces on the size-dependent elastic state of nano-inhomogeneities, Appl. Phys. Lett 82 (2003) 535.

[22] P. Sharma, S. Ganti, Size-dependent eshelby's tensor for embedded nano-Inclusions incorporating surface/interface energies, Journal of Applied Mechanics 71(5) (2004) 663-671.

[23] P. Sharma, L. T. Wheeler, Size-dependent elastic state of ellipsoidal nano-inclusions incorporating surface/interface tension, Journal of Applied Mechanics Vol. 74 (2007) 447.

[24] H. Duan, J. Wang, Z. Huang, B. Karihaloo, Eshelby formalism for nano-inhomogeneities, Proc. R. Soc. A 461 (2005) 3335–3353.

[25] H. Duan, J. Wang, Z. Huang, B. Karihaloo, Size-dependent effective elastic constants of solids containing nano-inhomogeneities with interface stress, Journal of the Mechanics and Physics of Solids 53 (7) (2005) 1574 – 1596. doi:DOI:10.1016/j.jmps.2005.02.009.

[26] Z. Hashin, The spherical inclusion with imperfect interface, Journal of Applied Mechanics 58 (2) (1991) 444–449. doi:10.1115/1.2897205.

[27] Z. Hashin, Thermoelastic properties of particulate composites with imperfect interface, Journal of the Mechanics and Physics of Solids 39 (6) (1991) 745 – 762. doi:http://dx.doi.org/10.1016/0022-5096(91)90023-H.

[28] J. Qu, The effect of slightly weakened interfaces on the overall elastic properties of composite materials, Mechanics of Materials 14 (4) (1993) 269 – 281. doi:http://dx.doi.org/10.1016/0167-6636(93)90082-3.

[29] J. Qu, Eshelby tensor for an elastic inclusion with slightly weakened interface, Journal of Applied Mechanics 60 (4) (1993) 1048–1050. doi:10.1115/1.2900974.

[30] Z. Zhong, S. A. Meguid, On the elastic field of a shpherical inhomogeneity with an imperfectly bonded interface, Journal of Elasticity 46 (2) (1997) 91–113. doi:10.1023/A:1007342605107.

[31] L. Nazarenko, H. Stolarski, H. Altenbach, Effective properties of short-fiber composites with gurtin-murdoch model of interphase, International Journal of Solids and Structures 97-98 (2016) 75 – 88. doi:http://dx.doi.org/10.1016/j.ijsolstr.2016.07.041.

[32] H. Yu, A new dislocation-like model for imperfect interfaces and their effect on load transfer, Composites Part A: Applied Science and Manufacturing 29 (9-10) (1998) 1057 – 1062. doi:http://dx.doi.org/10.1016/S1359-835X(98)00010-4.

[33] H. Yu, Y. Wei, F. Chiang, Load transfer at imperfect interfaces-dislocation-like model, International Journal of Engineering Science 40 (14) (2002) 1647 – 1662. doi:http://dx.doi.org/10.1016/S0020-7225(02)00028-9.

[34] Y. Zhao, G. Weng, Transversely isotropic moduli of two partially debonded composites, International Journal of Solids and Structures 34 (4) (1997) 493 – 507. doi:http://dx.doi.org/10.1016/S0020-7683(96)00027-3.

[35] Y. H. Zhao, G. J. Weng, The effect of debonding angle on the reduction of effective moduli of particle and fiber-reinforced composites, Journal of Applied Mechanics 69 (3) (2002) 292–302. doi:10.1115/1.1459068.

[36] P. H. Dederichs, R. Zeller, Variational treatment of the elastic constants of disordered materials, Zeitschrift fur Physik A Hadrons and Nuclei Volume 259, Number 2 (1973) 103-116, DOI: 10.1007/BF01392841.

[37] W. Azoti, Y. Koutsawa, A. Tchalla, A. Makradi, S. Belouettar, Micromechanics-based multi-site modeling of elastoplastic behavior of composite materials, International Journal of Solids and Structures 59 (2015) 198 – 207. doi:http://dx.doi.org/10.1016/j.ijsolstr.2015.02.002.

[38] W. Azoti, A. Tchalla, Y. Koutsawa, A. Makradi, G. Rauchs, S. Belouettar, H. Zahrouni, Mean-field constitutive modeling of elasto-plastic composites using two (2) incremental formulations, Composite Structures 105 (2013) 256–262. doi:10.1016/j.compstruct.2013.05.044.

[39] I. Doghri, A. Ouaar, Homogenization of two-phase elasto-plastic composite materials and structures: Study of tangent operators, cyclic plasticity and numerical algorithms, International Journal of Solids and Structures 40 (7) (2003) 1681 – 1712. doi:10.1016/S0020-7683(03)00013-1.

[40] P. Vieville, A. S. Bonnet, P. Lipinski, Modelling effective properties of composite materials using the inclusion concept. general considerations, Arch. Mech. 58 (3) (2006) 207–239.

[41] O. Fassi-Fehri, Le problème de la paire d'inclusions plastiques et hétérogènes dans une matrice anisotrope : Application à l'étude du comportement des matériaux composites et de la plasticité, Ph.D. thesis, Université de Metz (1985).

[42] J. D. Eshelby, The determination of the elastic field of an ellipsoidal inclusion, and related problems, Proceedings of the Royal Society of London. Series A, Mathematical and Physical Sciences 241 (1226) (1957) 376–396.

[43] J. Wang, H. Duan, Z. Zhang, Z. Huang, An anti-interpenetration model and connections between interphase and interface models in particle-reinforced composites, International Journal of Mechanical Sciences 47 (4-5) (2005) 701 – 718, a Special Issue in Honour of Professor Stephen R. Reid's 60th Birthday. doi:DOI:10.1016/j.ijmecsci.2004.12.014.

[44] Z. Hashin, Thin interphase/imperfect interface in elasticity with application to coated fiber composites, Journal of the Mechanics and Physics of Solids 50 (12) (2002) 2509 – 2537. doi:http://dx.doi.org/10.1016/S0022-5096(02)00050-9.

[45] M. Shokrieh, M. Esmkhani, Z. Shokrieh, Z. Zhao, Stiffness prediction of graphene nanoplatelet/epoxy nanocomposites by a combined molecular dynamics-micromechanics method, Computational Materials Science 92 (2014) 444 – 450. doi:http://dx.doi.org/10.1016/j.commatsci.2014.06.002.

[46] A. Elmarakbi, W. Jianhua, W. L. Azoti, Non-linear elastic moduli of graphene sheet-reinforced polymer composites, International Journal of Solids and Structures 81 (2015) 383–392doi:http://dx.doi.org/10.1016/j.ijsolstr.2015.12.019.

[47] D. Systemes, Abaqus 6.12 Example Problems Manual, Simulia.

Research Highlights

- The linear spring model is considered for studying the interfacial imperfection;
- The overall properties are derived by a modified Mori-Tanaka scheme;
- Numerical results are performed for a graphene platelets GPL reinforced polymer composite;
- A FE multiscale simulation is implemented on a GPL reinforced metal matrix composite.